Exchange Bias Effect in La 0.2 Ca 0.8 MnO 3 Antiferromagnetic Nanoparticles with Two Ferromagnetic-Like Contributions

ARTICLE *in* THE JOURNAL OF PHYSICAL CHEMISTRY C · FEBRUARY 2011

Impact Factor: 4.77 · DOI: 10.1021/jp109035n

THE JOURNAL OF PHYSICAL CHEMISTRY C

ARTICLE

pubs.acs.org/JPCC

Exchange Bias Effect in $La_{0.2}Ca_{0.8}MnO_3$ Antiferromagnetic Nanoparticles with Two Ferromagnetic-Like Contributions

Vladimir Markovich,*[,†] Roman Puzniak,[‡] Dmitrii Mogilyansky,[§] Xiaodong Wu,[∥] Kiyonori Suzuki,[∥] Ivan Fita,[‡,⊥] Andrzej Wisniewski,[‡] Shijian Chen,[∥] and Gad Gorodetsky[†]

[†]Department of Physics, Ben-Gurion University of the Negev, 84105 Beer-Sheva, Israel

[‡]Institute of Physics, Polish Academy of Sciences, Aleja Lotnikow 32/46, 02-668 Warsaw, Poland

[§]The Analytical Research Services and Instrumentation Unit, Ben-Gurion University of the Negev, 84105 Beer-Sheva, Israel

[∥]Department of Materials Engineering, Monash University, Clayton, Victoria 3800, Australia

[⊥]Donetsk Institute for Physics & Technology, National Academy of Sciences, 83114 Donetsk, Ukraine

ABSTRACT: We report the structural and magnetic properties of $La_{0.2}Ca_{0.8}MnO_3$ nanoparticles synthesized by a chemical route, having an average diameter of 15 nm. Synchrotron experiments performed in the temperature range 80−300 K have shown that below 200 K a structural transition from room temperature orthorhombic *Pnma* to monoclinic $P2_1/m$ space group, associated with orbital ordering, survives in studied particles, although this transition is highly suppressed in comparison with that of the bulk. The magnetization of these particles exhibits the appearance of a ferromagnetic contribution from the shell at $T > 200$ K, antiferromagnetic ordering within the particle core at $T_N \sim 140$ K, and the emergence of another ferromagnetic contribution at $T < 100$ K. The latter appears as a result of spin canting within the antiferromagnetic core or is developed at some interfaces inside the nanoparticles. Considerable horizontal (H_{EB}) and vertical (M_{Shift}) shifts of the magnetization hysteresis loops are observed after field cooling, manifesting the exchange bias (EB) effect. We found that a nonmonotonic variation of H_{EB} and M_{Shift} as well as of the coercive field (H_C) can be caused by the changes in the temperature at which the cooling field (H_{cool}) is applied. The maximum values of negative H_{EB} and positive M_{Shift} are obtained when $H_{cool} = 15$ kOe is applied between 100 and 200 K. Moreover, the exchange bias field, the remanent magnetization, the coercive field, as well as the magnitude of the vertical shift depend strongly on the magnitude of H_{cool}. Our studies show that the volume fraction of the ferromagnetic phase, the strength of the interfacial exchange, and the topology of phase separation are altered clearly by the procedure of application of the magnetic field. The existence of two interfaces contributing to the total EB effect is proposed to explain the observed effects.

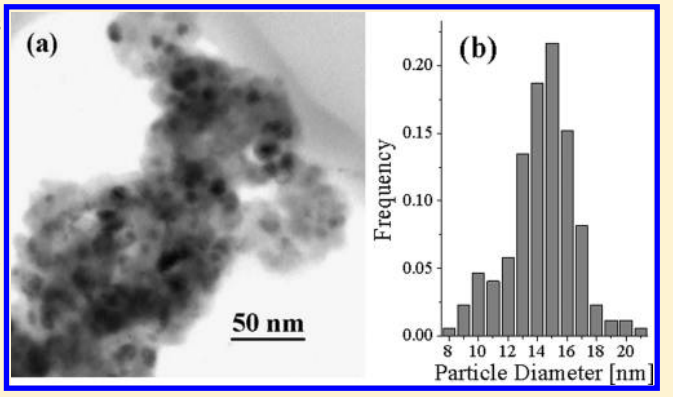

1. INTRODUCTION

The magnetism of antiferromagnetic (AFM) nanoparticles[1] is interesting predominantly due to their potential for exhibiting a magnetization reversal by quantum tunneling, their weak ferromagnetism below the Néel temperature T_N, and their potential for improvement of the permanent magnet quality.[2] Néel predicted[3] that AFM particles may have a small net magnetic moment due to an unequal number of spins on the two sublattices resulting from the finite size effect (see also ref 4). The breaking of a considerable number of exchange bonds between the surface atoms, a large surface/volume ratio, the surface roughness, and the breaking of the symmetry are only a few of the essential causes that can change the magnetic properties of small particles. It should be noted that the precise identification of the nature of the surface contribution remains unclear, and various terms used to describe its properties such as "disordered surface state" or "uncoupled spins" or "spin-glass-like behavior", etc. only underline the uncertainty in the description of the shell contribution.[5]

The hysteresis loops of AFM particles often exhibit the exchange bias (EB) effect when an AFM system with a surface ferromagnetic (FM) component is cooled in the magnetic field through T_N of the AFM phase. Most of the EB models[6] were developed for systems with $T_N < T_C$ (where T_C is Curie temperature of the FM component); however, the unconventional EB has been observed also in some systems with $T_N > T_C$.[7,8] In addition to traditional FM/AFM systems, the EB effect was also observed in samples containing a ferrimagnet (FI) or a spin-glass (SG) phase.[6] Recently, phenomenological models and Monte Carlo studies[9] have shown an enhancement of surface charge

Received: September 21, 2010
Revised: December 2, 2010
Published: December 30, 2010

density and confirmed a suppression of the antiferromagnetic charge ordered (AFM/CO) phase and an emergence of FM order with spin-glass-like behavior near the surface for AFM nanomanganites, resulting in a natural AFM/FM interface and the EB effect. This model is in agreement with recent studies of AFM nanoparticles of electron-doped manganites,[10−15] which suggest that at the surface of basically AFM manganite particles small FM clusters are formed within the disordered spin matrix.

Magnetic properties of nanoparticles are very sensitive to interparticle interactions.[16,17] The magnetic moments of AFM nanoparticles are typically much smaller than those of FM and FI ones, and the magnetic dipole interaction between AFM particles is usually negligible.[1] At high particle densities as shells come into contact and their effective thickness increase twice, apart from the classical dipole interaction, the exchange coupling between atoms belonging to neighboring particles starts to play a role in the system.[1,16,17] Correspondingly, Rozenberg et al.[18] proposed that electrons tunneling between two Mn ions located in adjacent manganite particles may induce FM double exchange (DE) correlations due to local spin polarization of these electrons, similarly to electron hopping between two Mn ions in the bulk. The presence of such an interparticle exchange interaction may have a considerable influence on the EB properties.

Recent studies of basically charge ordered $La_{1-x}Ca_xMnO_3$ ($x > 0.5$),[14,19,20] $Nd_{0.5}Ca_{0.5}MnO_3$,[21] $Pr_{0.65}Ca_{0.35}MnO_3$,[22] and $Pr_{0.5}Ca_{0.5}MnO_3$[13] nanoparticles have demonstrated relaxation effects of superexchange interaction in the surface layer and formation of a FM-like shell, whose thickness increases with decreasing particle size. It was found that by reducing the particle size surface effects dominate and suppress the CO. When the grain size is reduced below 40 nm, CO completely melts, and the core spin configuration changes from antiparallel arrangement to canted AFM through spin coupling.[13,21] It is well-known[23,24] that the CO transition is accompanied by structural transition, and it is also characterized by a peak in the magnetization where the double exchange is suppressed due to the localization of the charge carriers. Similarly to the CO phase, the orbital ordered (OO) phase in $La_{0.2}Ca_{0.8}MnO_3$ particles monotonously weakens with decreasing particle size,[25] though it still survives even in particles as small as 15 nm. Indeed, the temperature dependences of magnetization of $La_{0.2}Ca_{0.8}MnO_3$ particles with an average particle size of 15−37 nm show a size-dependent peak (at T_{OO} = 153 K for smaller 15 nm particles and T_{OO} = 201 K for larger 37 nm particles), and ac-susceptibility has a two-peak structure, where the high-temperature peak is associated with an establishment of the orbital ordered AFM state.[25] Such features are absent in basically charge-ordered $La_{1/3}Ca_{2/3}MnO_3$ nanoparticles with average particle size between 12 and 42 nm, and only one wide peak, associated with transition to the AFM state, shows up.[26] We suggest that the C-type AFM structure observed in bulk $La_{0.2}Ca_{0.8}MnO_3$ manganite is much more stable than that observed in $La_{1/3}Ca_{2/3}MnO_3$, resulting in survival of OO even in 15 nm $La_{0.2}Ca_{0.8}MnO_3$ particles and leading to a disappearance of any CO state in $La_{1/3}Ca_{2/3}MnO_3$ at particle size ≤42 nm.[26] It appears that $La_{0.2}Ca_{0.8}MnO_3$ particles are just a special case of AFM manganite nanoparticles. It is highly desirable to support conclusions of magnetization measurements[25] by the results obtained with other experimental techniques.

In this paper, we discuss magnetic properties and the EB effect in compacted uncoated $La_{0.2}Ca_{0.8}MnO_3$ particles with an average size of 15 nm, in which the presence of interparticle exchange interactions affects the EB properties. The coercive field, the exchange bias field, as well as the vertical shift of the hysteresis loops vary significantly depending on the protocol of the application of magnetic field, and they approach maximal values if the field during cooling is applied at $100 \leq T \leq 200$ K. This surprising behavior is suggested to originate from the changes of the shell magnetic properties when the application of magnetic field affects the topology and effective thickness of the shell. We have also studied the crystal structure of 15 nm nanoparticles and bulk $La_{0.2}Ca_{0.8}MnO_3$ samples using synchrotron X-ray powder diffraction to establish the interrelation of magnetic properties and structure.

2. EXPERIMENTAL SECTION

$La_{0.2}Ca_{0.8}MnO_3$ particles were prepared by the glycine-nitrate method, previously used for preparation of the nanosized $La_{0.7}Ca_{0.3}MnO_3$ powder.[27] The X-ray diffraction (XRD) pattern of the as-prepared sample presents a mixture of perovskite and amorphous phases. After annealing at T = 750 °C, a pure orthorhombic perovskite phase with the average crystallite sizes $\langle D \rangle = 15 \pm 1$ nm was obtained. The studied sample will be denoted herein by LCMO15. The size of the particles and their composition were confirmed by transmission electron microscopy (TEM), high-resolution TEM, and energy-dispersive X-ray spectroscopy (EDS) analysis.

In addition to the conventional room-temperature structural analysis,[25] we have employed a low-temperature synchrotron powder diffraction technique for structural investigation of bulk $La_{0.2}Ca_{0.8}MnO_3$ samples and LCMO15 to establish the role of the crystal structure played in tuning the physical properties of the $La_{0.2}Ca_{0.8}MnO_3$ nanoparticles. High-resolution synchrotron X-ray powder diffraction patterns were collected with the Mythen microstrip detector on the powder diffraction beamline at the Australian Synchrotron in Debye−Scherrer transmission configuration. Powder samples were sealed in low X-ray absorption glass capillaries (d = 0.3 mm) and rotated during measurements. Data were collected at selected temperatures between 80 and 300 K on heating, using X-rays with a wavelength of 0.82481 Å.

Cylinder-shaped samples having a diameter of 2.4 mm and height of 3.0 mm prepared by compaction of LCMO15 powder under a pressure of ∼5 kbar were used in magnetic studies. The measurements, using a Princeton Applied Research (model 4500) vibrating sample magnetometer, were completed in the temperature range 5−290 K and magnetic fields $H \leq 15$ kOe, while the measurements of ac-susceptibility in the temperature range 5−300 K as well as the measurements of magnetization in higher magnetic field were performed using the magnetic option of the Physical Property Measurement System of Quantum Design and a Quantum Design SQUID Magnetometer MPMS XL.

3. RESULTS AND DISCUSSION

The bright-field TEM image of LCMO15 powder dispersed in an alcohol and placed on a carbon grid is shown in Figure 1(a). The images show plenty of nearly spherical nanoparticles whose size distribution is given by the histogram shown in Figure 1(b), and the histogram was obtained by analyzing several frames of similar bright-field images. The high-resolution TEM image[25] of a single particle of LCMO15 has shown the single-phase lattice-resolved planes of almost spherical particles with an average size of 15 nm, which is in close agreement with the results obtained from XRD studies.

The X-ray synchrotron data were treated by the Rietveld analysis with FullProf program package[28] to obtain crystal structure

parameters. The profile of the diffraction line was fitted using a pseudo-Voigt function, and the background was approximated by a limited number of experimental points linearly interpolated for intermediate values. The original atomic positions and isotropic thermal factors for La/Ca atoms were taken from a previous report[23] and then were refined only for the bulk sample. The atomic positions and isotropic thermal factors for oxygen atoms were fixed for all samples in the course of the refinement procedure.

Figure 2(a,b,c,d) shows the representative experimental XRD scan and corresponding fit for bulk (a,c) and nano (b,d) samples at a temperature of 300 and 80 K, respectively. The crystal structure of both nano and bulk $La_{0.2}Ca_{0.8}MnO_3$ perovskite is orthorhombic at room temperature and described with the *Pnma* space group (Figure 2(a,b)) as was reported earlier.[25] It is well-known that at temperatures below 220 K the ceramic samples of $La_{0.2}Ca_{0.8}MnO_3$ undergo transition to the orbitally ordered state, and the crystallographic symmetry is reduced from orthorhombic *Pnma* to monoclinic $P2_1/m$ space group.[23,24] This effect is simply indicated on the XRD pattern for bulk sample by splitting of some reflections, and it becomes more visible at low temperatures because of an increase of the monoclinic angle β. Figure 2(c) shows the experimental and fitted data for the bulk sample at 80 K. All diffraction peaks were indexed in the monoclinic setting of the $P2_1/m$ space group.

The 80 and 300 K peak profiles for nano and bulk samples in the 2θ range limited from 57° to 60° are presented in Figure 3 (this region is marked in Figure 2 by a stroke line). At T = 300 K, the peak of the orthorhombic phase at 2θ = 58.5° (signed by (**a**)) consists of (602), (206), (444), and (282) almost overlapping reflections. The corresponding peak of the nano sample is symmetrically broadened. Due to monoclinic distortion, each orthorhombic reflection (*hkl*) from this group splits into (*hkl*) and ($\bar{h}kl$) reflections of the monoclinic phase. In the case of the bulk sample (see Figure 3(b)), monoclinic distortion and changes of the lattice parameters lead to the appearance of three diffraction peaks at 80 K signed by **a1**, **a2**, and **a3**. Peak **a1** is formed by ($\bar{4}44$), ($\bar{6}02$), and ($\bar{2}06$) reflections (exclusively monoclinic peak), peak **a2** by (206), ($\bar{2}82$), and (602) reflections, and peak **a3** by (282) and (444) reflections. In the case of the nanocrystal sample, the effect

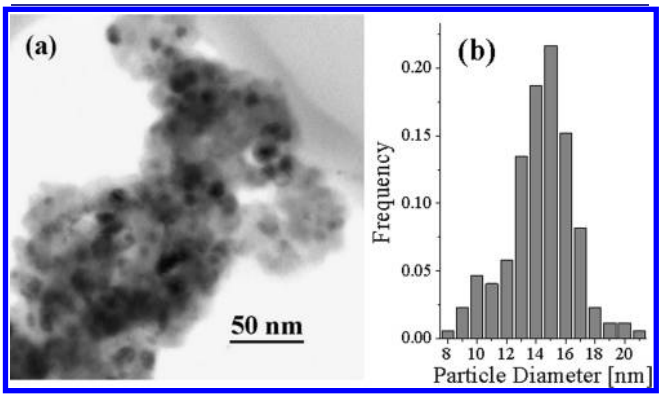

Figure 1. (a) Bright-field TEM image of a 15 nm $La_{0.2}Ca_{0.8}MnO_3$ sample. (b) The normalized histogram of particle size distribution.

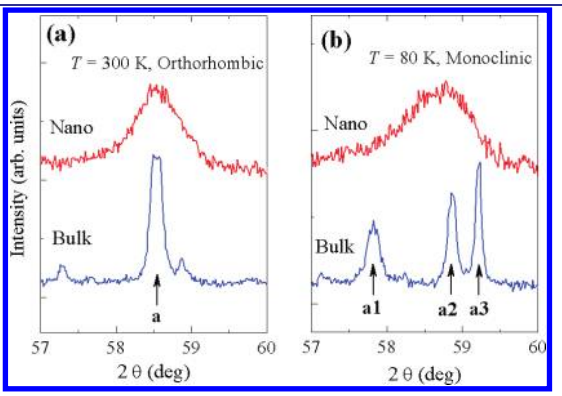

Figure 3. Peak profiles in the range 2θ = 57−60° for bulk and nano samples at 300 K (a) and 80 K (b) showing the splitting of the orthorhombic reflection due to monoclinic distortion.

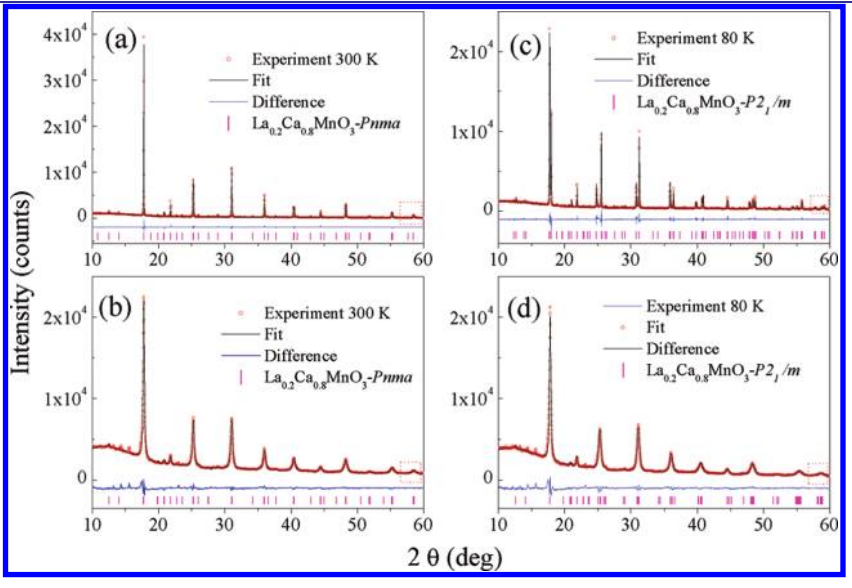

Figure 2. Rietveld plots for the bulk $La_{0.2}Ca_{0.8}MnO_3$ sample at 300 K (a) and 80 K (c) and for the 15 nm $La_{0.2}Ca_{0.8}MnO_3$ sample at 300 K (b) and 80 K (d). The data points are indicated by open circles, and the calculated and difference patterns are shown by solid lines. The Bragg positions of the reflections of manganite are indicated by vertical lines below the pattern.

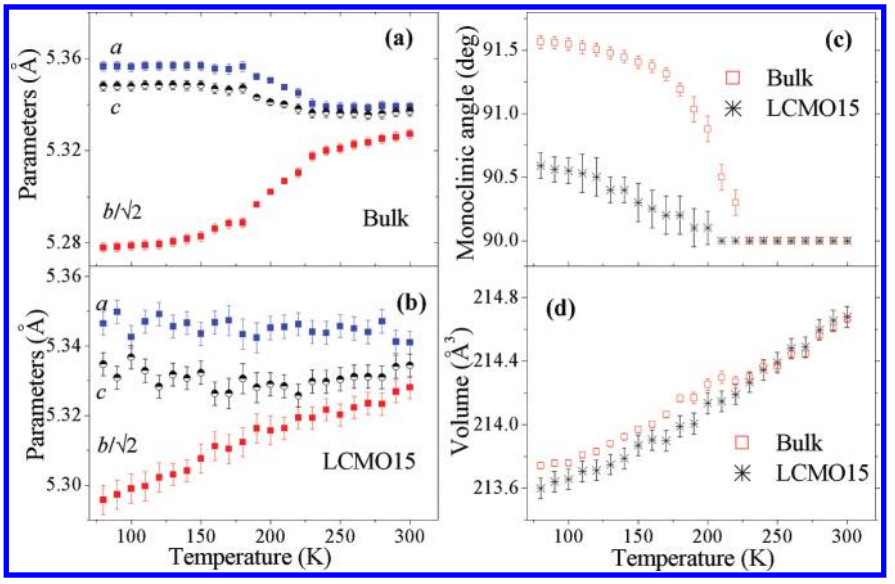

Figure 4. Temperature dependences of lattice parameters (a) and (b), monoclinic angle β (c), and unit cell volume (d) with the error bars for the bulk and nano samples.

of monoclinic splitting is not pronounced because of the great broadening of the diffraction peaks. However, it should be noted that the broadening of the presented diffraction peak at T = 80 K becomes more asymmetric as compared to that at T = 300 K, and this asymmetry is associated with the arrangement of splitted XRD peaks of the bulk sample that is demonstrated in Figure 3(b). This indicates that the monoclinic phase seems to be a more relevant structural description also for the nanocrystalline sample at low temperatures. The Rietveld plot for the nano sample at 80 K is shown in Figure 2(d).

Additionally, we performed the structure refinement of the diffraction experimental data for the nanocrystalline sample in the angular range of $2\theta = 30-82°$ using both orthorhombic *Pnma* and monoclinic $P2_1/m$ structural models. This angular region was chosen to diminish the errors caused by the highly nonlinear background at low diffraction angles. As a criterion for determination of the model relevance, we have used residual factors R_{wp} and R_{Bragg} of the Rietveld refinement. It was found that at temperatures below 150 K the monoclinic model gives R factors approximately 5−7% lower than the orthorhombic model. For example, at T = 80 K the R_{wp} = 3.7 and R_{Bragg}= 5.12 for the monoclinic model, and R_{wp} = 4.0 and R_{Bragg} = 5.65 for the orthorhombic model. Obviously, the monoclinic distortion was found to be considerably smaller for the nano sample than that for the bulk sample, and the monoclinic angle β even at the lowest measured temperatures deviates from 90° only by 0.5−0.6°. The deviation of the monoclinic angle β from 90° becomes too small in the temperature interval 150−210 K, and therefore, it is practically impossible to distinguish between these two models. Above 210 K, the orthorhombic structure is stable for both samples. All these variations are shown in Figure 4, where the temperature dependences of the lattice constants and monoclinic angle with corresponding error bars for the nanocrystalline sample (Figure 4(b,c)) as well as for the bulk sample (Figure 4(a,c)) are presented. In the same graph, the changes of the unit cell volume are shown (Figure 4(d)). The temperature behavior of the lattice constants and monoclinic angle for bulk samples (Figure 4(a,c)) is in agreement with the data reported earlier.[23] The lattice constants *a* and *c* remain essentially unchanged in the measured temperature range for the nanosample (Figure 4(b)), and only parameter *b* as well as the volume of the unit cell decrease with cooling.

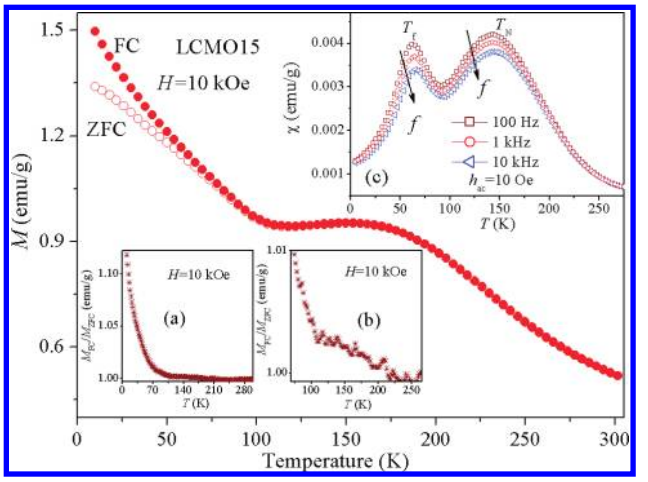

Figure 5. Temperature dependence of zero field cooled M_{ZFC} (open symbols) and field cooled M_{FC} (solid symbols) magnetization of the LCMO15 sample measured in magnetic field H = 10 kOe. Insets: (a) The temperature dependence of the ratio between the magnetization obtained after FC and ZFC, respectively; (b) the temperature dependence of the ratio between the magnetization obtained after FC and ZFC in the extended scale; and (c) temperature dependence of a real component of ac-susceptibility χ' of the LCMO15 sample measured during heating at different frequencies.

Field cooled (M_{FC}) and zero field cooled magnetization (M_{ZFC}) curves for LCMO15 samples, recorded at an applied field H = 10 kOe, are shown in Figure 5. It can be clearly seen that the remnant orbital ordering (OO) peak appears at $T \approx 153$ K in the 15 nm particles, while it is observed in bulk $La_{0.2}Ca_{0.8}MnO_3$ at $T_{OO} \approx 214$ K.[29,30] Both ZFC and FC magnetization curves start to diverge already at $T \sim 220$ K (see insets (a) and (b) in Figure 5). At $T < 100$ K, the magnetization exhibits a considerable increase, while ZFC and FC curves split further off, indicating the onset of a weak FM moment at T_C(on) ≈ 100 K, where the difference between ZFC and FC curves is a measure of irreversibility.

dx.doi.org/10.1021/jp109035n |*J. Phys. Chem. C* 2011, 115, 1582–1591

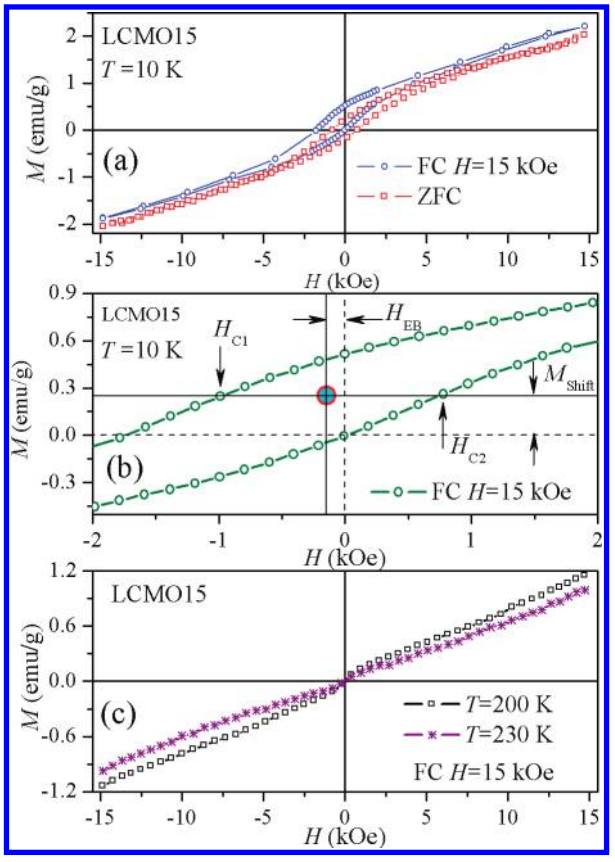

Figure 6. (a) Field dependence of magnetization of the LCMO15 sample at 10 K after ZFC and FC in $H = 15$ kOe. (b) The hysteresis loop measured at 10 K after FC with definitions of EB parameters. (c) Field dependence of magnetization at high temperatures after FC.

It was previously suggested, for bulk $La_{0.23}Ca_{0.77}MnO_3$, that the small net FM moment, that appears at $T_C \sim 64$ K, could correspond to a slight canting of the spins in a C-type AFM phase, or alternatively, this FM contribution appears at the interfaces between the charge ordered (CO) and charge disordered (CD) domains.[30]

The temperature dependence of ac-susceptibility of LCMO15 shows two peaks at temperatures 62 and 142 K (see inset (c) in Figure 5). The position of the peak at 142 K is independent of frequency, and it may be attributed to the Néel temperature T_N of the AFM core. The position of the low-temperature peak shifts to higher temperatures with increasing frequency, indicating slow spin dynamics. Such a behavior together with pronounced splitting between ZFC and FC magnetization may be associated with the freezing at temperature T_f of FM clusters which are formed within the disordered spin matrix at the surface of particles.[10,13,18] The spontaneous magnetization M_0 was evaluated by linear extrapolation of the high-field magnetization, measured in magnetic fields H up to 90 kOe (not shown), to $H = 0$, and it was found that M_0 for LCMO15 at 5 K is about 0.9 emu/g (0.026 μ_B/f.u.). Since the theoretical value of the magnetization for the fully ordered spins M_{theor} is 3.2 μ_B/f.u., we may roughly evaluate that the volume of the FM phase in LCMO15 is only about 0.8% at 5 K, and this small M_0 value originates mainly from the nanometer-sized FM clusters distributed within the disordered shell.

Magnetic hysteresis loops were measured at different temperatures after cooling in zero field (ZFC) and after cooling in an applied field (FC) of $H_{cool} = 15$ kOe. Figure 6(a) shows $M(H)$ curves recorded for the LCMO15 sample at 10 K after ZFC and FC. While the ZFC $M(H)$ loop is nearly centered at zero field, the FC one exhibits horizontal and vertical shifts, manifesting the phenomenon of exchange bias. The loop shift along the field axis in the EB systems shows up due to an energy barrier, which appears at the FM/AFM interface after field cooling. The significantly large vertical shift may be associated with uncompensated spins in the AFM component of frozen spins of EB systems.[6,31] It is known that the vertical shift in the EB systems depends on the cooling field and the microstructure of the AFM component.[31] In the absence of the vertical displacement, the exchange bias and coercive fields are defined as $H_{EB} = (H_{C1} + H_{C2})/2$ and $H_C = (H_{C2} - H_{C1})/2$, where H_{C1} and H_{C2} are coercive fields for decreasing and increasing the magnetic field. Since a significant vertical shift takes place, we have defined H_{EB} and H_C using the above relations, but with H_{C1} and H_{C2} obtained at intercepts of the loop with a horizontal line, which characterizes the vertical loop offset M_{Shift}[32] (see Figure 6(b)). The measurements of magnetization loops at various temperatures have shown that a spontaneous magnetization tentatively attributed to the presence of the FM phase is still observed up to 210 K. Only above this temperature $M(H)$ curves do not display spontaneous magnetization (see Figure 6(c)). The temperature variation of the exchange bias field H_{EB}, remanent magnetization, and spontaneous magnetic moment of $La_{0.2}Ca_{0.8}MnO_3$ nanoparticles with particle size of 15−37 nm was already discussed in terms of the magnetic coupling between the AFM core and the FM-like shell.[25] Another series of experiments provided additional information about the occurrence of the exchange bias in LCMO15 particles. Here, we followed the procedure originally developed by Gökemeijer and Chien[33] and recently used by Berkowitz et al.[34] The values of H_{EB}, H_C, and M_{Shift} were obtained from $M(H)$ loops recorded at 10 K after various cooling protocols (see Table 1 and Figure 7): (a) ZFC to the indicated temperatures and subsequent FC in 15 kOe to 10 K and (b) FC in 15 kOe to the indicated temperatures and subsequent ZFC to 10 K. Figure 7 and Table 1 present some noticeable features. First, the FC to indicated temperature Y shows that, as expected, maximal values of parameters are observed for FC to 10 K, and both H_{EB} and M_{Shift} monotonically decrease with increasing Y. This result shows that with decreasing Y a fraction of the interfacial spins at the shell that have been pinned along a direction compatible with the core/shell exchange interaction monotonically increases giving rise to the shift of the hysteresis loop. Second, the ZFC to the indicated temperature X with subsequent FC to 10 K shows that maximal values of H_{EB}, H_C, and M_{Shift}, which are even larger than those for FC from room temperature to 10 K, were obtained for $100 \leq X \leq 200$ K. This feature, which is surprising in itself, is to our knowledge absent in other systems.[33,34] The unexpected behavior may be connected with the specific magnetic structure of AFM manganite nanoparticles.

It should be noted that the EB is estimated from the hysteresis loop shift away from the zero-field axis for an effectively saturated system as the ascending and descending branches of the hysteresis loop coincide for fields higher than the anisotropy field.[6,8,35] However, the hysteresis loops presented in Figure 6 (a) are closed, and possible effects of the minor loop are rather very small when the exchange bias H_{EB} and coercive H_C fields are much smaller than the measuring field $H = 15$ kOe. Further evidence for a "true" exchange coupling and its manifestation such as occurrence of H_{EB} and M_{Shift} arises from the measurements of the hysteresis loops in the maximum applied field of 70 kOe. The

Table 1. Vertical Loop Offset (M_{Shift}), Exchange Bias (H_{EB}), and Coercive (H_C) Fields, after Different Field-Cooling Protocols

ZFC from 300 K to X K, then FC in 15 kOe to 10 K	FC from 300 K in 15 kOe to Y K, then ZFC to 10 K			
Y (K)	X (K)	M_{Shift} at 10 K (emu/g)	H_{EB} at 10 K (Oe)	H_C at 10 K (Oe)
200		0.27	−108	1029
140		0.27	−120	1045
100		0.256	−119	985
70		0.238	−89	971
40		0.185	−66	955
30		0.155	−47	948
20		0.088	−26	877
10		0.001	+14	853
	200	0.001	−15	829
	100	0.015	−27	826
	50	0.092	−59	853
	30	0.145	−97	795
	10	0.255	−99	848

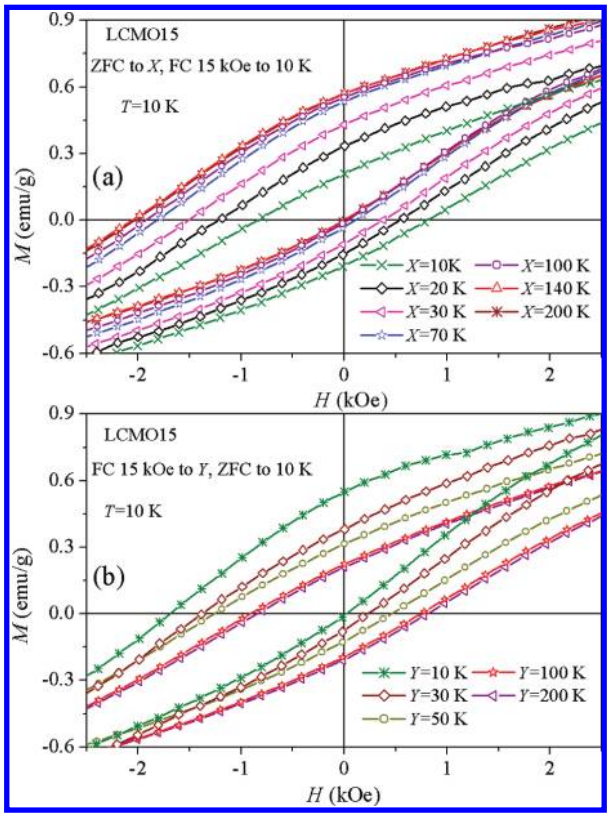

Figure 7. Hysteresis loops of the LCMO15 sample at 10 K after various cooling protocols: (a) ZFC to the indicated temperatures (X) and subsequent FC in 15 kOe to 10 K and (b) FC in 15 kOe to the indicated temperatures (Y) and subsequent ZFC to 10 K.

cooling field dependence H_{cool} of the EB effect was studied while the sample was cooled to 10 K from 300 K in different H_{cool} (0−70 kOe), and the hysteresis loops were measured between ±70 kOe (see Figure 8). In the inset to Figure 8, the low-field region is expanded. The H_{cool} dependences of H_{EB}, H_C, and M_{Shift} and remanence magnetization M_r are shown in the top

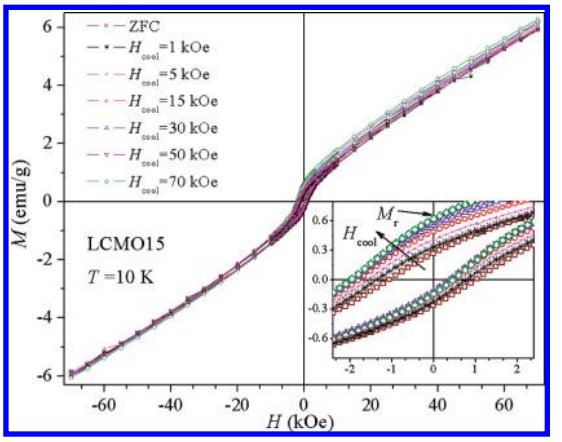

Figure 8. Hysteresis loops at T = 10 K of the LCMO15 sample cooled under various static fields with a measuring field ±70 kOe. The inset shows a magnified view of the central portion of the loops.

and bottom panels of Figure 9. With the increase of H_{cool}, the alignment of the moments of FM clusters along a preferential direction is enhanced, which reduces the effect of averaging of the anisotropy due to randomness.[36] The values of all the above parameters increase significantly with the increasing cooling field value up to H_{cool} = 5 kOe. At a higher H_{cool}, they exhibit quite different trends. Very similar variation of M_{Shift} and M_r with increasing H_{cool} (Figure 9(a)) shows that the increase of the vertical shift with increasing H_{cool} can be associated with the increasing number of magnetic moments frozen in the FC direction, which cannot be reversed by the applied field. As can be seen in Figure 9(a), upward M_{Shift} depends strongly on the cooling field. A careful analysis[31] of the relationship between vertical shift and interfacial coupling for AFM/FM (FeF_2−Fe and MnF_2−Fe) bilayers has shown that for a small cooling field M_{Shift} is upward or downward depending on the microstructure of the sample, while for large H_{cool} it is always upward since the interface coupling is overcome. The correlation between the low-field vertical shift M^0_{shift}(in Figure 9(a), M^0_{shift} is taken as a vertical shift for H_{cool} = 1 kOe) and the exchange bias is also found.[31] In particular, it

dx.doi.org/10.1021/jp109035n |J. Phys. Chem. C 2011, 115, 1582–1591

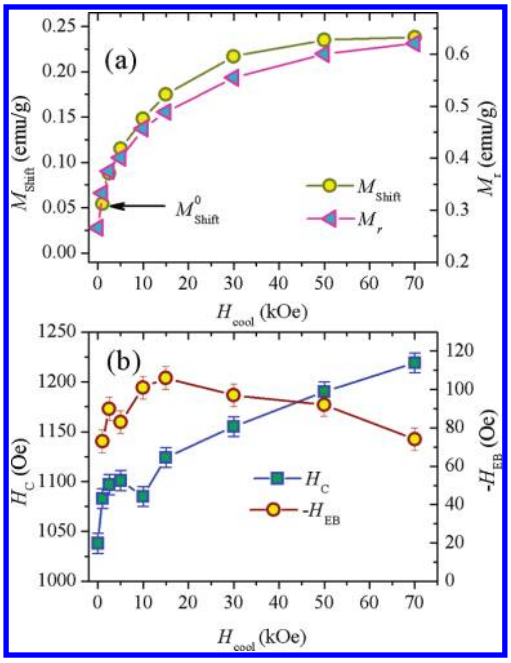

Figure 9. Variation of remanent magnetization M_r and vertical shift of M_{Shift} with field cooling H_{cool} (a). (b) Variation of coercive field and exchange bias field H_{EB} with field cooling H_{cool}.

was found[31] that samples with positive M^0_{shift} show almost no change in H_{EB} for any cooling field in qualitative agreement with our experimental results (see Figure 9).

An almost linear decrease in H_{EB} at $H_{cool} > 15$ kOe up to a maximal $H_{cool} = 70$ kOe (see Figure 9(b)) is reminiscent of the trend observed for the exchange biased systems involved with the SG state. In such systems, H_{EB} decreases considerably with increasing H_{cool} above a certain H_{cool} value. It is caused by large enough H_{cool} affecting the frozen spins in the SG phase as well as frozen FM spins.[36−40] For $H_{cool} < 5$ kOe, H_C increases changing from the ZFC value of ∼1040 to ∼1100 Oe at $H_{cool} = 5$ kOe, and then H_C exhibits a linear increase with increasing cooling field for $H_{cool} > 15$ kOe up to ∼1220 Oe for $H_{cool} = 70$ kOe. In contrast with the behavior of H_{EB}, H_C almost monotonously increases with increasing H_{cool} since its value is determined not only by the strength of magnetic interactions and topology of interfaces but also mainly by the intrinsic magnetic anisotropy of the system. It appears that with increasing alignment of the moments of FM clusters (Figure 9(a)) a higher field should be applied to reverse the magnetization. Such behavior of H_C is in contrast with that for systems involving spin-glass type of phases[36,39] and also for systems with FM/AFM[40] interfaces. The monotonic increase of H_C with increasing H_{cool} up to 16 kOe was observed only for $LaMn_{0.7}Fe_{0.3}O_3$ consisting of short-range FM clusters and the SG-like phase,[12] though the existence of the "true" EB effect in this compound seems to be doubtful.[35]

As pointed out already, recent studies of AFM nanoparticles[8−13] suggest a core−shell structure with the AFM core below T_N, while the shell may embody a spin-glass-like FM surface layer. The SG model of exchange bias may be relevant in this case. This model[41] includes few basic assumptions: (i) the FM/AFM interface is SG like; (ii) frozen uncompensated AFM spins are mainly responsible for the EB; and (iii) low anisotropy AFM spins contribute to coercivity. This model describing AFM nanoparticles suggests the presence of two types of AFM states, one with larger anisotropy and another, in the vicinity of the AFM/FM interface, with weaker anisotropy which allows some spins to rotate together with FM spins. It is commonly assumed that the pinned uncompensated spins belong to AFM, and the vertical shift observed in some nanoparticle systems has been found to be correlated with exchange bias and can be considered rather large to arise solely from uncompensated AFM spins.[6] Recent experimental results, obtained by a polarized neutron reflectometry study of FeF_2/Co (FM/AFM) bilayers[42] and by element-specific X-ray magnetic circular dichroism for FM/AFM/FM trilayers,[43] have shown, however, the presence of pinned uncompensated moments in both the FM and AFM layers.

In conventional exchange bias films, the thickness of the FM layer t_{FM} is fixed after fabrication and cannot be changed by H_{cool}, and the tuning of H_{EB} depends only on the change of the interfacial spins of FM and/or AF layers with the change of H_{cool}. In contrast to such EB systems, we may suggest in AFM manganite particles a possibility for tuning of the t_{FM} by external forces after fabrication due to a delicate balance of different ground states and strong competition among charge, spin, orbital, and lattice degrees of freedom. Upon cooling in H_{cool}, the external field can favor the process of growth of the FM phase, resulting in maximal t_{FM} as one cools the sample in H_{cool} from 300 to 10 K, while in the case of ZFC to the fixed temperature between 100 and 200 K and subsequent FC to 10 K, the effective thickness of spin-glass-like FM surface layers is somewhat reduced. Assuming that $H_{EB} \propto 1/t_{FM}$, the changes of t_{FM} with changes of H_{cool} may contribute to the unexpected behavior of the EB values with cooling protocols (see Table 1). It should be taken into account the existence of an interface between the small FM clusters in frustrated configuration and the interfacial AFM phase. Then the growth of the FM phase and possible transformation of some part of the AFM interfacial phase into an FM phase may also lead to a decrease of the number of FM/AFM interfaces, resulting in the decrease of the exchange energy and eventually in the decrease of H_{EB} and H_C at different cooling protocols.[6] Therefore, there are two different competing mechanisms leading to the nonmonotonic variation in the EB effect when temperature of application H_{cool} varies. It should be noted that the possibility of tuning the thickness of the FM layer by applied magnetic field was proposed recently for some bulk cobaltites and manganites involving interfaces between FM and SG regions[36,44,45] or between FM and AFM regions.[40]

The interpretation of the EB effect based on the picture of AFM core exchange coupled with an SG-like shell, which comprised small FM clusters, may be oversimplified in the case of LCMO15. Let us turn now to the possible magnetic structure of LCMO15. We note that neutron diffraction and magnetization studies of bulk $La_{1-x}Ca_xMnO_3$ ($0.5 \le x \le 0.9$) have shown that the phase diagram can be described with four stable distinct phases ($x = 1/2$, 2/3, 4/5, and 1) and a metastable ($x = 3/4$) phase.[46] Pissas and Kallias[46] have proposed also that in the range $2/3 \le x \le 4/5$ three phases coexist due to fluctuations which tend to stabilize the x=3/4 charge-ordered state. The phase coexistence has a rich manifestation in the time-dependent evolution of transport and magnetic properties observed recently for $La_{0.23}Ca_{0.77}MnO_3$ and related to the motion of the CO/CD structural interfaces.[30] Niebieskikwiat et al.[30] proposed that the small FM moment which appears in bulk $La_{0.23}Ca_{0.77}MnO_3$ is associated with interfaces between CO and CD domains. The appearance of the small FM-like contribution at $T \sim$ 70−100 K was observed for bulk electron-doped $La_{1-x}Ca_xMnO_3$ ($x \sim 0.75-0.8$)[27,29,30,46] and $Pr_{1/3}Ca_{2/3}MnO_3$[47] samples, and thus it is not a consequence of the nanodimension of

the particles. Therefore, this feature is not a nanoeffect since it was reported for the nanoparticles, as well as for bulk samples.

The existence of the spontaneous magnetization and spin-glass-like behavior in AFM manganite nanoparticles, (see Figure 6(c) and refs 25 and 26) at temperatures up to 200 K may be associated with some high-temperature magnetic ordering in the paramagnetic system of nanocrystals, i.e., with the appearance of spin clusters having net magnetic moments. This ordering probably appears due to a strong influence of surfaces and interparticle interactions on the system properties. It is well-known that for ferro- and ferrimagnetic particles both magnetic dipole−dipole interactions and exchange interactions play a key role.[1,17] In contrast, for AFM and weakly ferromagnetic particles, exchange coupling between the surface atoms of neighboring particles may be the most important interaction.[1,17] A specific kind of magnetic interparticle interaction, which significantly contributes to the formation of some collective state in ensembles of AFM manganite nanoparticles and high-temperature ordering at the surface, arises from a plausible mechanism recently proposed by Rozenberg et al.[18] It was suggested that electrons tunneling between two Mn ions located in adjacent manganite nanoparticles may induce FM DE correlations due to local spin polarization of these electrons, similarly to electron hopping between two Mn ions in the bulk. It was also suggested that the same effect leads to a surface clustering at temperatures below which thermal fluctuations are unable to destroy local FM clusters.[18] The DE correlations across the interface between two neighboring manganite nanoparticles are likely to be even stronger than the bulk counterpart due to dangling of some of Mn−O−Mn bonds on the grain surfaces.[18] Consequently, the FM-correlated spin clusters of low concentration appear at the contact interfaces between neighboring grains. Spatial frustration of nanoparticles in an ensemble of nanoparticles results in randomization of FM moments and formation of the spin-glass-like state at high temperatures.[18]

Since bulk $La_{0.2}Ca_{0.8}MnO_3$ does not exhibit any spin-glass-like features,[24] our observations suggest that spin-glass-like behavior is mostly attributed to the surface layer similarly to many other AFM and FM oxide nanoparticles.[48,49] Nevertheless, the presence of a specific mechanism of interparticle interactions in the case of the manganite nanoparticle[18] may introduce particular manifestations of spin-glass-like properties. Note that proper study of glassy behavior should include relaxation, aging, and memory effects in ZFC and FC magnetization. We have recently studied these effects in compacted 18 nm $La_{0.8}Ca_{0.2}MnO_3$ manganite particles, showing the formation of a collective state in the ensemble of interacting ferromagnetic manganite nanoparticles in which superspin-glass (SSG) features coexist with superferromagnetic-like behavior.[50] It should be stressed also that studies of such effects in AFM nanoparticles are quite rare.[51] Furthermore, it should be noted that we observed recently unusual or even enigmatic time dynamics in AFM manganite nanoparticles[25,27] which represent more complex relaxation phenomena than that usually observed in spin glass or SSG systems. It is clear that further experimental work should be devoted to clarify these interesting issues.

It is generally accepted that in the case of a mixed FM−AFM state the magnetization isotherms represent a superposition of a high-field linear part typical for the AFM phase, and nonzero spontaneous magnetization appears due to the FM phase.[47,52] To determine the magnetic contribution of the AFM component, the high-field susceptibility of LCMO15 was evaluated by linear

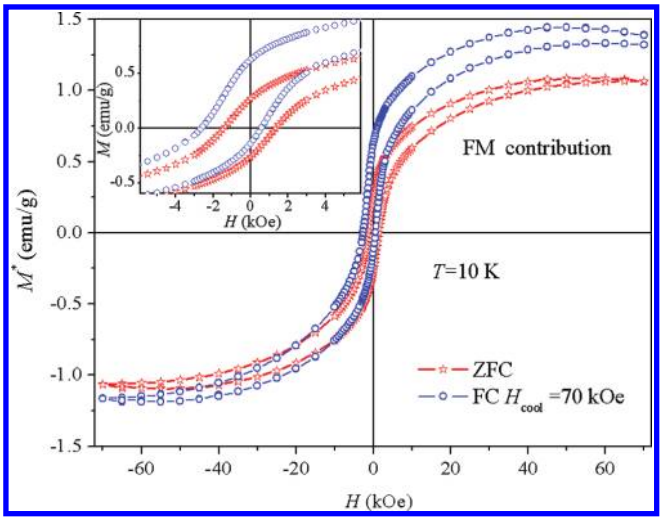

Figure 10. Resulting magnetization M^* vs H loop, after subtracting the contribution of the AFM core at $T = 10$ K for ZFC and FC at $H_{cool} = 70$ kOe. Inset shows low-field part of the M^* vs H loop.

extrapolation of ZFC $M(H)$ dependence (Figure 8) in the field range of 40−70 kOe. It was found that $\chi_{hf} = 6.89 \times 10^{-5}$ emu/g Oe. The development of the FM component becomes evident in Figure 10, where we show the resulting magnetization $M^*(H)$ after subtracting the linear background $M_{AFM} = \chi_{hf}H$ for both ZFC and FC (H_{cool} = 70 kOe) magnetization loops. Though FM-like magnetization should saturate in the magnetic field of a few kOe, the M^* does not saturate up to H as high as 40 kOe (see Figure 10). Possibly, this behavior may be related with the presence of the SG-like phase or alternatively with field-induced transformation between different magnetic phases. It should be noted that very similar behavior was previously observed for the bulk $Pr_{1/3}Ca_{2/3}MnO_3$ sample,[47] and it was related to the intrinsic coexistence of different magnetic phases.

Since both CO and CD phases are structurally different, this suggests the presence of strong martensitic strains at the CO/CD interfaces.[30] It is worth noting that OO phase in $La_{0.2}Ca_{0.8}MnO_3$ particles monotonously weakens with decreasing particle size,[25] though it still survives even in LCMO15, as is evidenced in the temperature variation of magnetization (see Figure 5) as well as in a temperature variation of lattice parameters (Figure 4). A reasonable hypothesis, leading to an explanation of the observed phenomenon, is to assume the presence of two interfaces contributing to the EB effect, namely, the first interface formed between basically the AFM and SG-like shell which comprises FM clusters in frustrated configuration and the second one formed inside the AFM core at the CO/CD interfaces. It has to be emphasized that one cannot provide an absolute proof for the existence of two interfaces and of two contributions to the EB effect from our magnetometric data. However, significant thermal and field dependence of the EB effect (Table 1 and Figures 9 and 10) may be associated with the presence of two interfaces. In particular, the significant increase of M_{Shift}, M_r, and H_C with increasing cooling field (Figure 9) can be explained partly by the martensite-like transition between CO and CD phases. Then, the increase of H_{cool} favors a small FM moment associated with the CD volume at the expense of the CO phase. Nonetheless, this FM moment remains particularly pinned during the recording of the descending branch of the hysteresis loops due to induced strong martensite strains.[30] Therefore, the domain boundary

motion necessarily implies atom displacements,[30] and an additional energy/magnetic field is needed to reverse the magnetization. It has been suggested that charge ordering and orbital ordering transitions in manganites are a martensitic-like transformation,[53,54] and peculiar field-induced metamagnetic transitions in charge and orbital ordered manganites may be explained in the frame of such a martensitic scenario.[54] During martensitic transformation, the deformation of the crystal lattice results in so-called accommodation strain, induced due to the nucleation of the martensitic particles within the parent crystal. It is known that the possibility to accommodate the martensitic strain decreases as the grain size of the polycrystalline sample decreases, and such an accommodation is especially not easy for nanoparticles.[55] Nevertheless, the survival of OO in LCMO15 (Figure 5) and the field-induced transformation from the remnant OO phase to the FM phase (Figure 10) support the assumption of the martensite-like scenario. Certainly, the manifestation of the martensitic-like scenario is less pronounced for nanosamples, and it may result only in relatively small variation of M^* with increasing magnetic field (Figure 10). In bulk CO/OO manganites, successive huge jumps of magnetization as a staircase effect in metamagnetic transitions were observed.[54] In the work of Biswas and Das,[22] the observed charge ordering in nanocrystalline $Pr_{0.65}Ca_{0.35}MnO_3$ with an average particle size of 36 nm, well visible in susceptibility and heat capacity, was attributed to the primary role played by the martensitic character of the charge order transition.

4. CONCLUSIONS

We have studied, in detail, the effect of size reduction on the crystal structure and magnetic properties of $La_{0.2}Ca_{0.8}MnO_3$ nanoparticles with average particle size of 15 nm. We show that, contrary to charge-ordered manganites, orbital ordering and concomitant structural transition from the room-temperature orthorhombic *Pnma* to low-temperature monoclinic $P2_1/m$ structure still survive in 15 nm $La_{0.2}Ca_{0.8}MnO_3$ particles. Moreover, we provide the evidence of surface effects and intrinsic interface exchange coupling in compacted 15 nm $La_{0.2}Ca_{0.8}MnO_3$ nanoparticles. Our results suggest the coexistence of a predominant AFM phase ($T_N \sim 140$ K) in the core with a minor FM component at the particle surfaces ($T < 220$ K) and a second FM component inside the AFM core. The compacted LCMO15 nanoparticles show horizontal and vertical shifts of magnetic hysteresis loops attributed to the exchange bias. We found a nonmonotonic variation of H_{EB} and M_{Shift} as well as a coercive field (H_C) at a variation in the temperature at which the cooling field H_{cool} was applied. Interestingly, the maximum values of H_{EB} and M_{Shift} were obtained when $H_{cool} = 15$ kOe was applied between 100 and 200 K. Results obtained suggest that the volume of the FM phase and the interfacial topology depend significantly on the protocol of application of the cooling field. Furthermore, the horizontal and vertical shifts of the hysteresis loops as well as the remanence and coercivity depend significantly on the magnitude of the cooling field. We suggest the presence of two interfaces with two-exchange coupling which contribute to the total EB effect.

AUTHOR INFORMATION

Corresponding Author

*Tel.: (+ 972 8 6477127). Fax: (+ 972 8 6472903). E-mail: markoviv@bgu.ac.il.

ACKNOWLEDGMENT

This work was supported in part by the Polish Ministry of Science and Higher Education under a research project no. N 202 1037 36. We thank L. Titelman for his help in the preparation of LCMO15 nanoparticles. The authors are indebted to Prof. J. Nogués for valuable discussions. The synchrotron experiment was carried out on the Powder Diffraction beamline at the Australian Synchrotron, Victoria, Australia. We thank Drs. K. Wallwork and Q. Gu for their expert advice on the synchrotron experiment.

REFERENCES

(1) Mørup, S.; Madsen, D. E.; Frandsen, C.; Bahl, C. R. H.; Hansen, M. F. *J. Phys.: Condens. Matter* **2007**, *19*, 213202.
(2) Sort, J.; Suriñach, S.; Muñoz, J. S.; Baró, M. D.; Nogués, J.; Chouteau, G.; Skumryev, V.; Hadjipanayis, G. C. *Phys. Rev. B* **2002**, *65*, 174420.
(3) Néel, L. In *Low Temperature Physics*; Dewitt, C., Dreyfus, B., de Gennes, P. G., Eds.; Gordon and Beach: New York, 1962.
(4) Kodama, R. H. *J. Magn. Magn. Mater.* **1999**, *200*, 359.
(5) Benitez, M. J.; Petracic, O.; Salabas, E. L.; Radu, F.; Tüysüz, H.; Schüth, F.; Zabel, H. *Phys. Rev. Lett.* **2008**, *101*, 097206.
(6) Nogués, J.; Sort, J.; Langlais, V.; Skumryev, V.; Suriñach, S.; Muñoz, J. S.; Baró, M. D. *Phys. Rep.* **2005**, *422*, 65.
(7) (a) Wu, X. W.; Chien, C. L. *Phys. Rev. Lett.* **1998**, *81*, 2795. (b) Cai, J. W.; Liu, Kai; Chien, C. L. *Phys. Rev. B* **1999**, *60*, 72.
(8) Salazar-Alvarez, G.; Sort, J.; Suriñach, S.; Baro, M. D.; Nogués, J. *J. Am. Chem. Soc.* **2007**, *129*, 9102.
(9) (a) Dong, S.; Gao, F.; Wang, Z. Q.; Liu, J.-M.; Ren, Z. F. *Appl. Phys. Lett.* **2007**, *90*, 082508. (b) Dong, S.; Yu, R.; Yunoki, S.; Liu, J. M.; Dagotto, E. *Phys. Rev. B* **2008**, *78*, 064414.
(10) Markovich, V.; Fita, I.; Wisniewski, A.; Puzniak, R.; Mogilyansky, D.; Titelman, L.; Vradman, L.; Herskowitz, M.; Gorodetsky, G. *Phys. Rev. B* **2008**, *77*, 054410.
(11) Huang, X. H.; Ding, J. F.; Zhang, G. Q.; Hou, Y.; Yao, Y. P.; Li, X. G. *Phys. Rev. B* **2008**, *78*, 224408.
(12) Thakur, M.; Patra, M.; De, K.; Majumdar, S.; Giri, S. *J. Phys.: Condens. Matter* **2008**, *20*, 195215.
(13) Zhang, T.; Dressel, M. *Phys. Rev. B* **2009**, *80*, 014435.
(14) Zhang, T.; Zhou, T. F.; Qian, T.; Li, X. G. *Phys. Rev. B* **2007**, *76*, 174415.
(15) Zhang, T.; Wang, X. P.; Fang, Q. F. *J. Phys. Chem. C* **2010**, *114*, 11796.
(16) Nogués, J.; Skumryev, V.; Sort, J.; Stoyanov, S.; Givord, D. *Phys. Rev. Lett.* **2006**, *97*, 157203.
(17) Hansen, M. F.; Koch, C. B.; Mørup, S. *Phys. Rev. B* **2000**, *62*, 1124.
(18) Rozenberg, E.; Shames, A. I.; Auslender, M.; Jung, G.; Felner, I.; Sinha, J.; Banerjee, S. S.; Mogilyansky, D.; Sominski, E.; Gedanken, A.; Mukovskii, Ya. M.; Gorodetsky, G. *Phys. Rev. B* **2007**, *76*, 214429.
(19) Sarkar, T.; Ghosh, B.; Raychaudhuri, A. K.; Chatterji, T. *Phys. Rev. B* **2008**, *77*, 235112.
(20) Lu, C. L.; Dong, S.; Wang, K. F.; Gao, F.; Li, P. L.; Lv, L. Y.; Liu, J. M. *Appl. Phys. Lett.* **2007**, *91*, 032502.
(21) Rao, S. S.; Tripathi, S.; Pandey, D.; Bhat, S. V. *Phys. Rev. B* **2006**, *74*, 144416.
(22) Biswas, A.; Das, I. *Phys. Rev. B* **2006**, *74*, 172405.
(23) Pissas, M.; Kallias, G.; Hofmann, M.; Többens, D. M. *Phys. Rev. B* **2002**, *65*, 064413.
(24) (a) Ling, C. D.; Granado, E.; Neumeier, J. J.; Lynn, J. W.; Argyriou, D. N. *Phys. Rev. B* **2003**, *68*, 134439. (b) Granado, E.; Ling, C. D.; Neumeier, J. J.; Lynn, J. W.; Argyriou, D. N. *Phys. Rev. B* **2003**, *68*, 134440.
(25) Markovich, V.; Fita, I.; Wisniewski, A.; Mogilyansky, D.; Puzniak, R.; Titelman, L.; Martin, C.; Gorodetsky, G. *Phys. Rev. B* **2010**, *81*, 094428.
(26) Markovich, V.; Fita, I.; Wisniewski, A.; Mogilyansky, D.; Puzniak, R.; Titelman, L.; Gorodetsky, G. *J. Appl. Phys.* **2010**, *108*, 063918.

(27) Markovic, D.; Kusigerski, V.; Tadic, M.; Blanusa, J.; Antisari, M. V.; Spasojevic, V. *Scripta Materialia* **2008,** *59*, 35.
(28) Rodríguez-Carvajal, J. *Phys. B* **1993,** *192*, 55.
(29) Markovich, V.; Fita, I.; Puzniak, R.; Rozenberg, E.; Martin, C.; Wisniewski, A.; Yuzhelevski, Y.; Gorodetsky, G. *Phys. Rev. B* **2005,** *71*, 134427.
(30) (a) Tao, J.; Niebieskikwiat, D.; Salamon, M. B.; Zuo, J. M. *Phys. Rev. Lett.* **2005,** *94*, 147206. (b) Niebieskikwiat, D.; Tao, J.; Zuo, J. M.; Salamon, M. B. *Phys. Rev. B* **2008,** *78*, 014434.
(31) Nogués, J.; Leighton, C.; Schuller, I. K. *Phys. Rev. B* **2000,** *61*, 1315.
(32) Panagiotopoulos, I.; Basina, G.; Alexandrakis, V.; Devlin, E.; Hadjipanayis, G.; Colak, L.; Niarchos, D.; Tzitzios, V. *J. Phys. Chem. C* **2009,** *113*, 14609.
(33) Gökemeijer, N. J.; Chien, C. L. *J. Appl. Phys.* **1999,** *85*, 5516.
(34) Berkowitz, A. E.; Rodriguez, G. F.; Hong, J. I.; An, K.; Hyeon, T.; Agarwal, N.; Smith, D. J.; Fullerton, E. E. *Phys. Rev. B* **2008,** *77*, 024403.
(35) (a) Geshev, J. *J. Magn. Magn. Mater.* **2008,** *320*, 600. (b) Geshev, J. *J. Phys.: Condens. Matter* **2009,** *21*, 078001.
(36) Karmakar, S.; Taran, S.; Bose, E.; Chaudhuri, B. K.; Sun, C. P.; Huang, C. L.; Yang, H. D. *Phys. Rev. B* **2008,** *77*, 144409.
(37) Patra, M.; Thakur, M.; Majumdar, S.; Giri, S. *J. Phys.: Condens. Matter* **2009,** *21*, 236004.
(38) Passamani, E. C.; Larica, C.; Marques, C.; Takeuchi, A. Y.; Proveti, J. R.; Favre-Nicolin, E. *J. Magn. Magn. Mater.* **2007,** *314*, 21.
(39) (a) Del Bianco, L.; Fiorani, D.; Testa, A. M.; Bonetti, E.; Signorini, L. *Phys. Rev. B* **2004,** *70*, 052401. (b) Del Bianco, L.; Fiorani, D.; Testa, A. M.; Bonetti, E. *J. Magn. Magn. Mater.* **2005,** *290*−*291*, 102.
(40) Qian, T.; Li, G.; Zhang, T.; Zhou, T. F.; Xiang, X. Q.; Kang, X. W.; Li, X. G. *Appl. Phys. Lett.* **2007,** *90*, 012503.
(41) Radu, F.; Zabel, H. In *Magnetic Heterostructures: Advances and Perspectives in Spinstructures and Spintransport*; Zabel, H., Bader, S. D., Eds.; Springer Tracts in ModernPhysics; Springer-Verlag: Berlin, 2008; Vol. 227, pp 97−184.
(42) Fitzsimmons, M. R.; Kirby, B. J.; Roy, S.; Li, Z.-P.; Roshchin, I. V.; Sinha, S. K.; Schuller, I. K. *Phys. Rev. B* **2007,** *75*, 214412.
(43) Nogués, J.; Stepanow, S.; Bollero, A.; Sort, J.; Dieny, B.; Nolting, F.; Gambardella, P. *Appl. Phys. Lett.* **2009,** *95*, 152515.
(44) (a) Tang, Y.; Sun, Y.; Cheng, Z. *J. Appl. Phys.* **2006,** *100*, 023914. (b) Tang, Y. K.; Sun, Y.; Cheng, Z. *Phys. Rev. B* **2006,** *73*, 174419.
(45) Ang, R.; Sun, Y. P.; Luo, X.; Hao, C. Y.; Zhu, X. B.; Song, W. H. *J. Appl. Phys.* **2008,** *104*, 023914.
(46) Pissas, M.; Kallias, G. *Phys. Rev. B* **2003,** *68*, 134414.
(47) Niebieskikwiat, D.; Salamon, M. B. *Phys. Rev. B* **2005,** *72*, 174422.
(48) Kodama, R. H.; Berkowitz, A. E. *Phys. Rev. B* **1999,** *59*, 6321.
(49) Salazar-Alvarez, G.; Qin, J.; Šepelák, V.; Bergmann, I.; Vasilakaki, M.; Trohidou, K. N.; Ardisson, J. D.; A.; Macedo, W. A.; Mikhaylova, M.; Muhammed, M.; Baró, M. D.; Nogués, J. *J. Am. Chem. Soc.* **2008,** *130*, 13234.
(50) Markovich, V.; Fita, I.; Wisniewski, A.; Jung, G.; Mogilyansky, D.; Puzniak, R.; Titelman, L.; Gorodetsky, G. *Phys. Rev. B* **2010,** *81*, 134440.
(51) Mishra, S. K. *Eur. Phys. J. B* **2010,** *78*, 65.
(52) Koroleva, L. I.; Szymczak, R. *J. Phys. Chem. Solids* **2003,** *64*, 1565.
(53) Podzorov, V.; Kim, B. G.; Kiryukhin, V.; Gershenson, M. E.; Cheong, S.-W. *Phys. Rev. B* **2001,** *64*, 140406(R).
(54) (a) Hardy, V.; Hébert, S.; Maignan, A.; Martin, C.; Hervieu, M.; Raveau, B. *J. Magn. Magn. Mater.* **2003,** *264*, 183. (b) Hardy, V.; Majumdar, S.; Crowe, S. J.; Lees, M. R.; Paul, D. McK.; Hervé, L.; Maignan, A.; Hébert, S.; Martin, C.; Yaicle, C.; Hervieu, M.; Raveau, B. *Phys. Rev. B* **2004,** *69*, 020407(R).
(55) Zenji, N. In *Martensitic Transformation*; Fine, M., Meshii, M., Wayman, C., Eds.; Academic: New York, 1978.